Journal of Membrane Science 364 (2010) 157–166

Contents lists available at ScienceDirect

Journal of Membrane Science

journal homepage: www.elsevier.com/locate/memsci

Dynamics of an osmotic backwash cycle

Guy Ramon*, Yehuda Agnon, Carlos Dosoretz

Department of Civil and Environmental Engineering, Technion-Israel Institute of Technology, Haifa 32000, Israel

ARTICLE INFO

Article history:
Received 8 June 2010
Received in revised form 3 August 2010
Accepted 6 August 2010
Available online 13 August 2010

Keywords:
Reverse osmosis
Membrane cleaning
Osmotic backwash
Concentration polarization
Numerical simulation

ABSTRACT

Recent studies have provided preliminary indication that an osmotic-induced backwash of RO membranes may offer an innovative, effective and potentially chemical-free cleaning method. In this paper, we present numerical simulations of the two-dimensional, transient concentration field during an osmotic backwash event. Presented results illustrate the dynamics of the de-polarization process, permeation rate and characteristic time-scales, as influenced by various transport mechanisms present. Different possible configurations for inducing the osmotic backwash are considered, illustrating possible advantages and shortcomings. For a backwash cycle initiated by reduction of the trans-membrane pressure, it is shown that during short times, the backwash process is only weakly affected by the presence of a crossflow velocity, whereas it is this axial advection mechanism which strongly influences the permeation rate at longer times. For an osmotic backwash induced by injection of a high concentration 'draw' solution, it is shown that the pulse duration should be longer than the residence time for a maximum achievable cycle-averaged permeation rate. A shorter pulse is significantly diluted, particularly on the membrane surface, to the point where its concentration may drop below that required for inducing osmotic flow. Consequently, the pulse concentration and duration must be carefully optimized if efficient osmotic cleaning is to be achieved throughout the full length of a membrane train.

1. Introduction

Membrane-based desalting, such as reverse osmosis (RO), is considered world-wide as the most promising technology for potable water production from sea and brackish waters and wastewater reclamation. However, the efficiency of this process is severely hampered by concentration polarization (CP) and fouling; specifically, mineral scaling, adsorption of organic molecules, colloidal cake formation or the deposition and growth of biofilm-forming bacteria on the membrane surface significantly reduces productivity, resulting in increased energy consumption and shortened membrane life.

Pressure-driven backwashing is common practice in filtration processes, including micro- and ultrafiltration, offering an effective means of fouling control; however, it is not employed for membranes used in desalting, as the high back-pressure required for a hydraulically driven backwash may rupture the composite membranes used (see, for example, [1]). Consequently, fouling of these membranes is addressed through extensive pretreatment and periodic chemical cleaning and disinfection [2–4]. These methods are of limited efficiency, and also constitute additional waste streams which must be properly disposed of.

The idea of employing an osmotic driving force for backwashing was proposed nearly three decades ago [5]. Osmotic backwashing may be induced when the feed-side osmotic pressure exceeds the applied hydraulic pressure across the membrane. This may be accomplished in several ways: reducing the feed-side applied pressure; equilibrating the trans-membrane-pressure by raising the permeate-side pressure (the permeate-side pressure may still be slightly lower than the feed-side hydraulic pressure, so as not to jeopardize membrane integrity), or injecting the feed channel with a pulse of a high concentration solution (an osmotic 'draw' solution). Each of these scenarios may have its pros and cons, both in terms of efficiency as well as implications for large scale implementation.

To date, there have been very few reported studies on the efficiency of osmotic backwashing, and these have been of a very macroscopic nature, employing commercial membrane elements [6–9]. These studies have illustrated the general dynamics of the backwash process, primarily through the monitoring of permeation rates and accumulated volume. More importantly, these studies have demonstrated the potential for removal of foulants from the membrane surface. For example, Sagiv and Semiat [6] performed experiments with super-saturated solutions of $CaCO_3$ and showed that backwash events, during which the flow and pressure in the feed were halted, may be used to restore the permeation rate. However, in their experiment, the flux decline was minimal over the period examined (5%) and so their claim requires further scrutiny

* Corresponding author.
E-mail address: ramong@tx.technion.ac.il (G. Ramon).

0376-7388/$ – see front matter © 2010 Elsevier B.V. All rights reserved.
doi:10.1016/j.memsci.2010.08.008

in the presence of a larger impact on the permeation; furthermore, under such conditions, it is unclear whether this flux decline is to be attributed to scaling rather than CP. In a recent study, Qin et al. employed a high concentration pulse for inducing an osmotic backwash in an RO system used to desalt secondary-treated wastewater [9]. They observed a rise in the turbidity of the brine stream during such an event (from 0.6 to 5 NTU), indicative of foulant removal from the membrane surface. It is unclear what was the nature of the removed material, which may have consisted of colloidal matter or biofilm deposited on the membrane. Despite these uncertainties, the described studies provide a preliminary indication regarding the potential for employing an osmotic backwash for membrane cleaning.

A model able to predict the time dependent water permeation during an osmotic backwash cycle is desirable if the process is to be optimized. As water production is halted during a backwash cycle, and permeate is "wasted", it is clear that a backwash cycle should be of as short a duration as possible, while still achieving the process goal of cleaning the membrane surface of accumulated salt precipitates, colloidal cake or biofilm. It is also worth noting that as fouling phenomena, particularly mineral scaling, exhibit a time-dependence in terms of formation kinetics and consolidation, the correct frequency of applying a backwash cycle is also of great importance, and may result in easier removal of foulants. Predictive models are important in achieving a general understanding of the process dynamics, providing quantitative insight on various parameters involved, particularly as to the permeation rates and time-scales.

A simplified model has been shown to quite accurately predict the late backwash stage, i.e. the steady permeation expected to be established as the concentration field becomes constant within the feed space. Transport of solute away from the membrane surface by water entering the feed space from the permeate side has been implicitly neglected, and a mass-transfer correlation was used to describe the feed-side transport [6]. Experimental results have shown that the permeation rate is greatly affected by this transport mechanism and cannot be ignored if a full backwash cycle is to be predicted. In particular, the transient stage must greatly depend on the osmotic flow; however, the full model requires the solution of a 2D, transient advection–diffusion equation which may only be achieved numerically. More recently, a model has been put forward for prediction of the fully transient osmotic flow and concentration profiles [8]. The presented model was reduced to a 1D transient diffusion equation through scaling arguments and introduction of an adjustable parameter which accounts for the advection associated with the osmotic-driven permeation. This parameter was extracted from experiments carried out with a commercial spiral-wound module, producing good agreement between model predictions and measurements. However, due to its semi-empirical nature this model is of limited value in addressing the process dynamics in a general context.

In this study, we present numerical simulations of an osmotic backwash event during a representative RO operation. These simulations demonstrate, through various parameters, the process dynamics, providing insight regarding the permeation rates and time-scales involved. In particular, the model is used to illustrate the characteristics of different backwash configurations.

2. Computational model

In order to gain insight of the backwash process, numerical simulations have been made using the finite-element software package, Comsol 3.5a. The model solves the partial differential equation describing the convection and diffusion in the feed channel, coupled with the membrane transport equation.

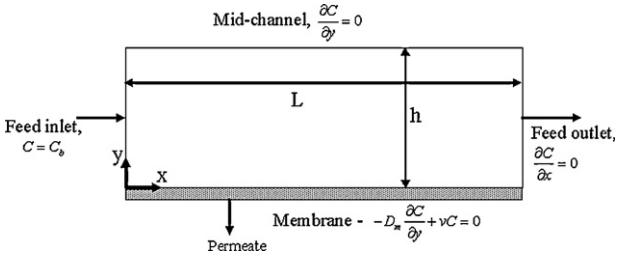

Fig. 1. Schematic drawing of the model domain.

The computational domain used in the simulations is a parallel-plate geometry, as depicted schematically in Fig. 1. It is bounded by upper and lower membrane walls, as well as the feed inlet/outlet boundaries. Owing to symmetry, only the bottom half of the channel is considered, thereby reducing the computational requirements. The model is two-dimensional, assuming that the third dimension (the channel width) is sufficiently large.

2.1. Model equations

The governing equation is obtained via a differential solute mass balance in the feed channel, resulting in the following 2D advection–diffusion equation:

$$\frac{\partial c}{\partial t}+u\frac{\partial c}{\partial x}+v\frac{\partial c}{\partial y}=D_m\left(\frac{\partial^2 c}{\partial x^2}+\frac{\partial^2 c}{\partial y^2}\right) \quad (1)$$

where $c(x,y,t)$ is the solute concentration and D_m is the solute molecular diffusion coefficient. x and y denote the axial and transverse coordinates, respectively, t is the time and u and v are the axial and transverse velocity components, respectively.

2.2. Boundary conditions

The following boundary conditions are imposed:
At the feed channel inlet, a constant concentration is imposed,

$$c(x=0,y,t)=c_b. \quad (2)$$

At the outlet, it is assumed that advection dominates diffusion, hence

$$\frac{\partial c}{\partial x}=0, \quad x=L. \quad (3)$$

The membrane is considered to be fully retentive, therefore

$$-D_m\frac{\partial c}{\partial y}+vc=0, \quad y=0. \quad (4)$$

Finally, we specify a symmetry condition at the mid-channel plane,

$$\frac{\partial c}{\partial y}=0, \quad y=h. \quad (5)$$

The approximation of a fully retentive membrane is an obvious idealization. The permeate concentration is not zero and so, during an osmotic backwashing event, salt rejected by the membrane accumulates on the permeate side; this concentration polarization is further aggravated by the fact that the only transport mechanism opposing this accumulation is molecular diffusion which is retarded within the membrane's porous support ('internal concentration polarization'). However, for a membrane with high salt rejection ($R>99\%$) this effect does not substantially alter the permeation rate, as will be shown in a later section.

Table 1
Physical properties and process parameters, used in the simulations.

h [mm]	L [m]	D_m [m^2/s]	C_b [M]	L_p [m/s Pa]	ΔP [MPa]
0.5	0.5	1.2×10^{-9}	0.5	3.4×10^{-12}	6

2.3. Velocity field

In general, the velocity components u and v must be obtained from the simultaneous solution of Eq. (1) along with the equation of continuity and the momentum balance equations (Navier–Stokes equations); these are coupled through the velocity field. However, a significant computational simplification may be obtained by considering a fully developed velocity profile. In particular, for the transient simulations performed in this study, inclusion of the Navier–Stokes equations resulted in convergence problems and exceedingly long simulation times.

Therefore, in this approximation, the axial component of the velocity field is given by

$$u(y) = UY(1 - Y) \tag{6}$$

where U is the channel centerline velocity and $Y = 2y/h$ is a scaled transverse coordinate, with h denoting half the channel height.

The transverse component of the velocity is the permeation rate, which we express using a linear osmotic pressure model, as follows:

$$-v = j = L_p(\Delta P - \beta \Delta c), \tag{7}$$

in which L_p denotes the membrane water permeability, ΔP is the trans-membrane pressure drop, $\beta = 2R_gT$ where R_g is the universal gas constant, and T is the absolute temperature. $\Delta c = c_m - c_p$ is the concentration difference across the membrane with c_m and c_p, denoting the membrane surface concentrations at the feed and permeate sides, respectively. It should be noted that, in order to ascertain the validity of this approximated velocity field, a comparison was made with the fully coupled solution of the Navier–Stokes equations, exhibiting a deviation of 1–2% in terms of the channel-averaged membrane surface concentration. In light of the significantly better convergence and lower computation intensity, this error was considered tolerable.

2.4. Process parameters

Values for various system parameters and physical properties used in the simulations are summarized in Table 1. These were chosen as representative of an RO process operating at room temperature. For each simulation run, the following quantities were computed:

The channel-averaged membrane surface concentration,

$$C_m = \frac{1}{L}\int_0^L c_m \, \mathrm{d}x, \tag{8}$$

the domain-average concentration within the channel,

$$C_d = \frac{1}{hL}\int_0^L \int_0^h c \, \mathrm{d}x \, \mathrm{d}y, \tag{9}$$

and the channel-averaged permeation rate,

$$J = \frac{1}{L}\int_0^L j \, \mathrm{d}x. \tag{10}$$

Where applicable, concentrations are scaled using the bulk concentration.

2.5. Computation details

The model domain was meshed using the mapped meshing function, generating 5000 rectangular elements. Due to the anticipated boundary layer characteristics of the concentration field, an asymmetric mesh was used, becoming exponentially finer at the membrane surface. The mesh was refined so as to eliminate oscillations in the transverse concentration profile, until further refinement did not yield improved results. Simulation times varied between ~5 and 30 min, depending on time-stepping convergence, on an Intel dual-core 1.66 GHz processor.

3. Results and discussion

In the following, results obtained from the numerical simulations will be presented, in which various aspects of the process dynamics will be elucidated. Two scenarios are considered for initiating a backwash cycle:

1. The trans-membrane pressure (ΔP) is equilibrated across the membrane, with (CF+) or without (CF−) the presence of crossflow.
2. A pulse of a high concentration osmotic solution is injected into the feed channel.

The initial condition for each simulation is a corresponding steady-state RO concentration field. The applied pressure, ΔP, is then set to zero and a backwash cycle simulation commences. In the case of an injected pulse, U and ΔP are left unchanged and an inlet concentration condition is adjusted according to the required pulse.

3.1. Model validation

In order to assess the accuracy of the numerical model, a comparison has been made with published experimental data of an osmotic backwash process. It should be noted that, since all published data has been obtained using commercial spiral-wound elements, a full comparison is not possible. This is due to the fact that the numerical model does not account for the (computationally expensive) complex velocity field in a spacer-filled channel. Nevertheless, the model has been validated for the case where a backwash cycle is induced by stopping the feed channel flow (i.e. $U = 0$, $\Delta P = 0$) where, in the absence of crossflow, the flow-field becomes trivial. Experimental data points were taken from Sagiv et al. [8] (experiment 20–40) and calculations were made using the corresponding experimental conditions. In particular, initial conditions were chosen such that the initial osmotic permeation rate matches the experimental value. As may be seen in Fig. 2, the model predictions agree very well with experimental results. Note that two simulations are illustrated: one with an 'ideal' fully retentive membrane and one with a 'leaky' membrane (modeled with a salt permeability of 2.5×10^{-7} m/s [10]). The two cases are virtually indistinguishable at short times, with the 'leaky' calculation providing a somewhat better agreement with the experimental data, for longer times. This is due to concentration polarization on the permeate side, and will be discussed further in the following section.

3.2. Effect of membrane rejection on osmotic permeation

Next, the time evolution of the osmotic-induced permeation is examined, as affected by a non-zero permeate concentration. For this simulation, an additional model domain is specified, in which an advection–diffusion equation is solved, coupled to

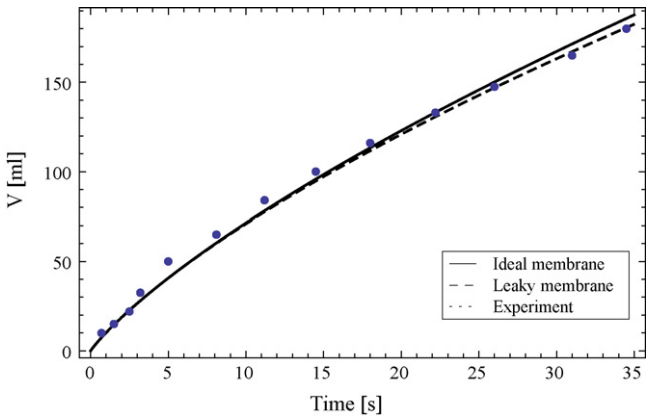

Fig. 2. Accumulated permeate volume, V, during an osmotic backwash event. Data points were taken from Sagiv et al. [8] (experiment 20–40). Model calculations were made with the corresponding process conditions: solid line – ideal, fully rejecting membrane; dashed line – 'leaky membrane' with a salt permeability of 2.5×10^{-7} m/s [10].

the feed domain through the permeation rate (dependent on the concentrations at domain boundaries corresponding with the membrane surface). In the permeate domain, there is no crossflow and the solute diffusion process occurs primarily within the membrane's porous support; this has a retarding effect which is approximated by specifying an 'effective' diffusion coefficient which is smaller than the 'free' diffusivity. Simulations were performed for various values of the observed membrane rejection, $R = 1 - c_p/c_b$, with no crossflow in the feed channel (see Fig. 3).

These simulations indicate that internal polarization may certainly have an impact on the evolution of the permeation rate, which becomes more pronounced as time progresses. After 50 s (which may be considered to be quite a long period), permeation with a membrane rejection of $R = 0.98$ is roughly 6% lower than that of an ideal membrane ($R = 1$), while for a higher rejection the effect becomes barely distinguishable. It may therefore be concluded, based on these results, that for a highly rejecting membrane, permeate-side polarization does not significantly impact the osmotic permeation. That being said, we do note that if a lower rejection membrane is in use, a significant reduction of the osmotic driving force may be expected (~19% at $R = 0.95$). This observation served as justification for performing the following simulations with the assumption of a fully retentive membrane, eliminating

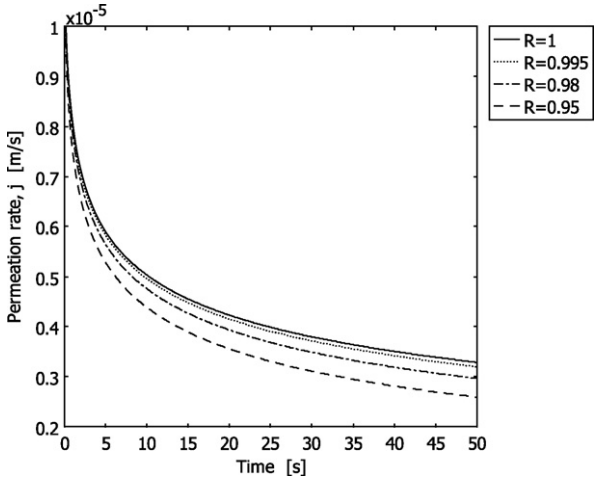

Fig. 3. Transient, averaged permeation rate calculated for various values of the membrane rejection, R. Simulations made with no crossflow ($U = 0$).

the need for solving two coupled domains and thus lowering the computational requirements.

3.3. CP boundary layer dissipation

Before turning to discuss the time evolution of the process, it is instructive to observe the different characteristics demonstrated by the dissipation of a CP layer by molecular diffusion, as opposed to the combined diffusion–advection in the presence of an osmotic back-flow. To this end, simulations have been carried out in the absence of a crossflow velocity, so that only transverse transport is accounted for. Fig. 4 is a representative case, where an identical CP layer undergoes diffusive dissipation in the presence (b) and absence (a) of the osmotically induced permeation; a third simulation is performed, in which an applied crossflow velocity $U = 0.5$ m/s is included, but without the osmotic permeation (c). We note that this velocity corresponds with the initial condition imposed on all three cases.

As may be seen, two features are immediately apparent; the first is, as may well be expected, the disparate time-scales involved. Diffusive dissipation requires ~25 s in order to reach a scaled surface concentration of $C_m/C_b \sim 1.1$, while in the presence of an osmotic back-flow, this surface concentration is reached within ~0.5 s. The second, and perhaps more interesting, feature is the shape of the concentration distribution.

In the diffusive case, the maximum concentration is always located at the membrane surface, and the profile dissipates from a sharp, exponential, distribution which flattens gradually. Under the influence of the osmotic flow, the CP layer is simultaneously detached from the membrane surface as it is diffusively dissipated. This 'traveling wave' behavior is characteristic of advection–diffusion processes, where, in this case, the advective velocity declines rapidly, concurrent with the surface concentration which drives it. However, this diffusive dissipation occurs faster since it now does so in two directions, as the front advances away from the membrane surface. This characteristic behavior has previously been shown for concentration de-polarization in the presence of a back-flow [8,11]. In the case where axial advection is added (Fig. 4c), the concentration profile resembles that of a purely diffusive process; however, dissipation occurs far more rapidly (~6 s to a flattened profile). This is a classical boundary layer result, whereby the diffusive dissipation is hydrodynamically 'confined' to a region adjacent to the solid boundary, which has the overall effect of maintaining higher transverse concentration gradients and, consequently, quicker dissipation.

Now, when a crossflow velocity is applied in the presence of osmotic permeation, an additional advective mechanism contributes to the dissipation of the CP layer. In this case, the characteristic shape of the concentration distribution is unchanged; however, the time-scales involved are somewhat reduced as the velocity increases. This may clearly be seen in Fig. 5, where the concentration profile is plotted at different times for velocities ranging between 0.05 and 0.5 m/s.

It must be noted that, for consistency, the initial concentration distribution for each case shown corresponds with the steady state achieved under the applied crossflow velocity. Thus, at low velocities, the initial surface concentration is higher than that for the high velocities. A higher surface concentration results in a larger driving force for the osmotic permeation, which would suggest a faster backwash cycle for the low crossflow case. However, it may be seen that the time required for the surface concentration to reach a value of $C_m/C_b \sim 0.8$ is reduced from ~4.5 s when $U = 0.05$ m/s, to ~2.3 s when $U = 0.05$ m/s despite the different initial concentrations. In their paper, Sagiv et al. [8] reasoned that at a high initial concentration, the higher osmotic flow rate induced a rapid dilution of the surface concentration, which in turn reduced the permeation

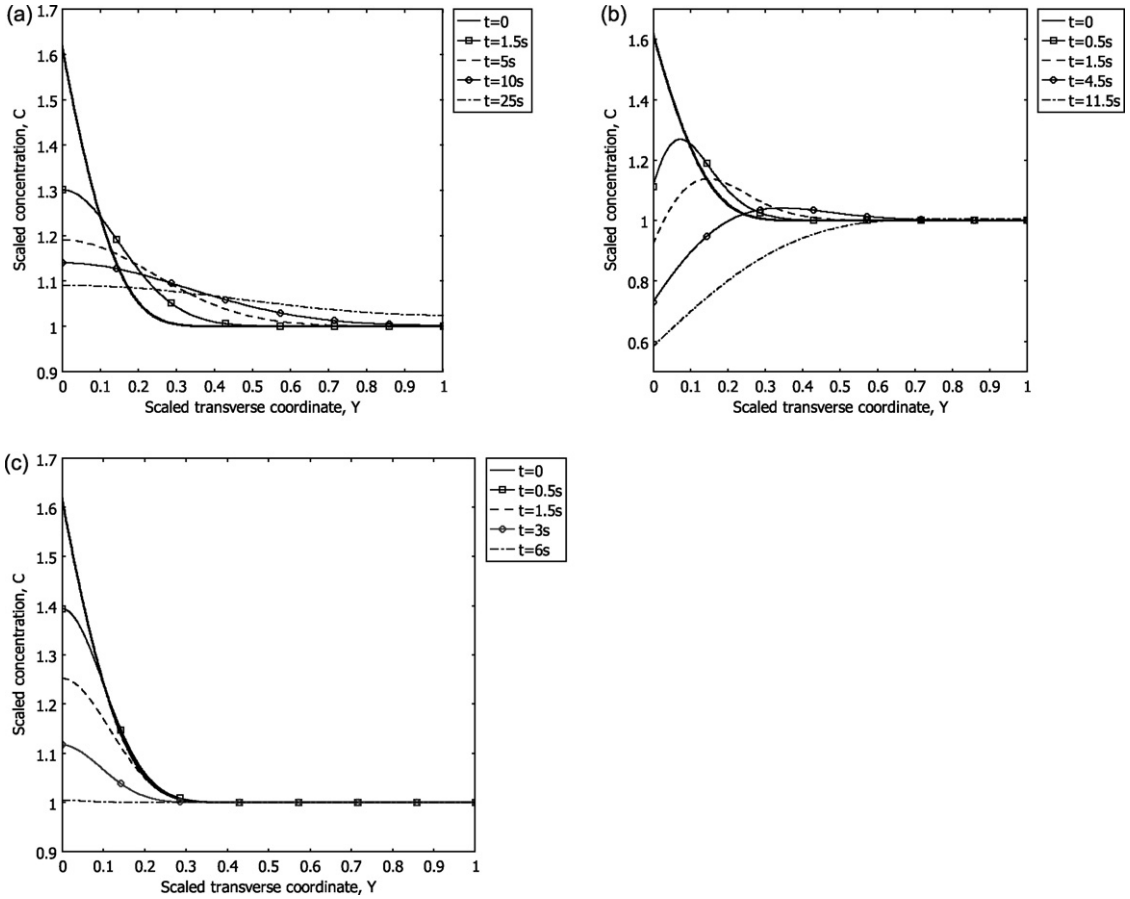

Fig. 4. Dissipation of the concentration polarization layer. (a) Diffusive dissipation (no crossflow/osmotic permeation). (b) Osmotic permeation (no crossflow). (c) Full process, $U = 0.25$ m/s.

rate. While this is indeed plausible, simulated results also indicate an impact of the axial advection on the dilution process (in the presence of crossflow), particularly at longer times. This is to be expected since the CP boundary layer thickness is dictated primarily by hydrodynamic conditions within the membrane channel. It may be also be seen, however, that at short times it appears that the dominant mechanism is indeed the osmotic permeation, as indicated by practically identical concentration profiles regardless of the crossflow velocity. We note that, while solute properties were not varied in the performed simulations, it is expected that these characteristics would remain unchanged, with a more dramatic impact of the osmotic flow in the case of a low diffusivity solute.

The transient concentration field within the feed channel is shown over a full dissipation process, for a velocity of $U = 0.25$ m/s (Fig. 6). The initial concentration field corresponds with the steady state achieved under the applied pressure and crossflow velocity, and clearly demonstrates classical boundary layer characteristics, as it develops along the channel length.

At $t = 0$, the TMP is reduced to zero, and the osmotic permeation commences. The CP layer seems to 'turn over', during the backwash process, as the concentration front detaches from the membrane surface out into the main stream, where it is carried away by the crossflow. A new, diluted, boundary layer is then established, in place of the concentrated one. This cycle takes place during the course of ~19 s for $U = 0.05$ m/s, and only ~6 s when $U = 0.5$ m/s.

3.4. Backwash characteristics

We now turn to examine various bulk properties of the process. First, it would be instructive to compare the backwash characteristics with and without the presence of the crossflow. The choice of either configuration would have direct technical consequences and therefore its pros and cons must be weighed carefully. Key features to this understanding are the time-scales involved. In their paper, Sagiv et al. [8] defined the end of a backwash cycle as the point where the concentration distribution becomes monotonic, i.e. the maximum concentration has completely flattened. We note that, at such a time, the surface concentration is well below the bulk concentration ($C_m/C_b \sim 0.8$ in the case considered); we denote this time as T_F. We further define two more time-scales; the time required for the membrane surface concentration to reach that of the bulk solution, T_M, and the time required to reach a steady state, T_S. The latter was defined as the point where changes in the membrane surface concentrations became smaller than 0.1%. We also note that in the case where significant permeate-side polarization is present, no steady state exists; however, as will be shown, this approximate steady-state time is useful when assessing the effect of the crossflow velocity on the backwash cycle.

The characteristic times are shown in Fig. 7, as a function of the crossflow velocity, U, in the range 0.05–0.5 m/s. We note that the calculations do not include the case of a zero crossflow velocity – this is due to the fact that in all other cases, the initial condition is consistent with the velocity present, and so a choice of initial condition for the no-crossflow case becomes arbitrary. Immediately apparent is the strong dependence of the time required for reaching a steady osmotic permeation, T_S, on the crossflow velocity applied. Conversely, the time T_M, required for reducing the membrane surface concentration to the bulk value, is only weakly affected by the presence of axial advection. As already mentioned, it appears

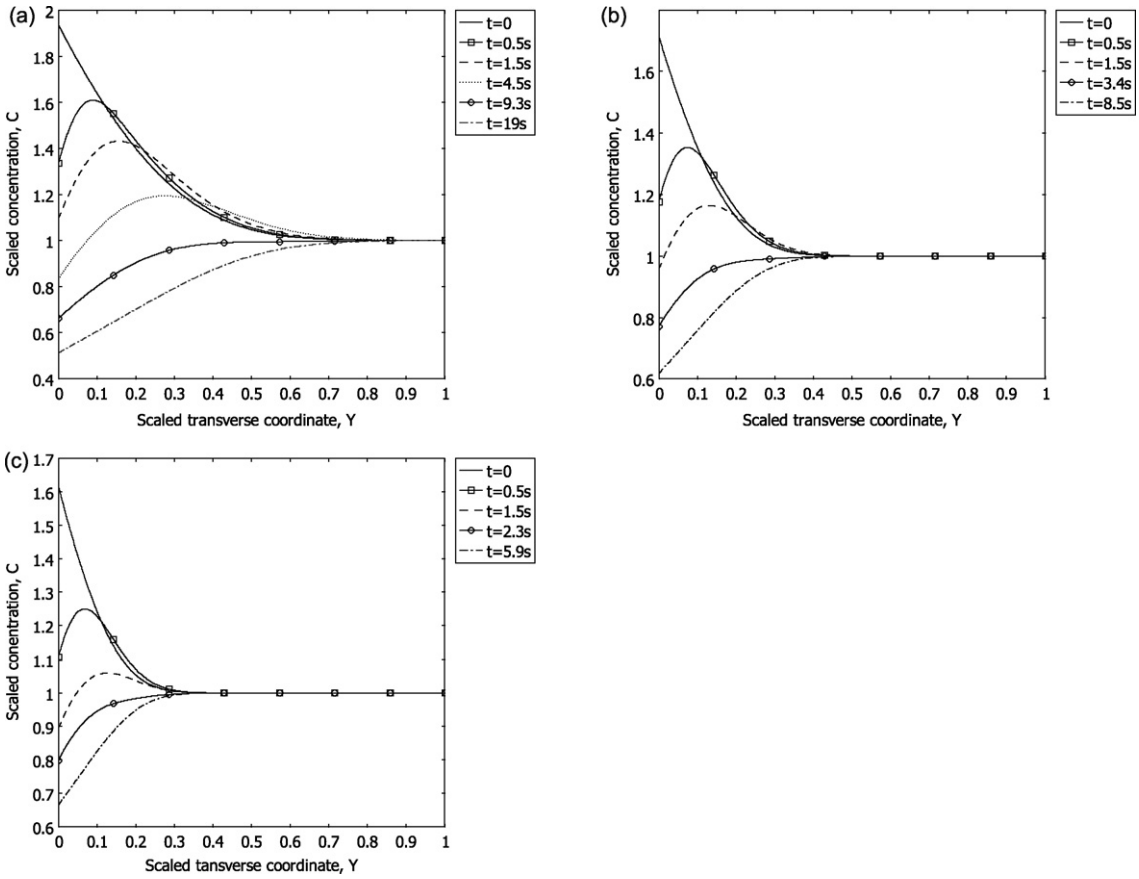

Fig. 5. Dissipation of the concentration polarization layer, with varying crossflow velocities. (a) $U = 0.05$ m/s. (b) $U = 0.25$ m/s. (c) $U = 0.5$ m/s.

that at shorter times the dominant mechanism responsible for depolarization is the osmotic permeation, while longer times are controlled by the crossflow. This may be understood in terms of the boundary layer character of the mass-transfer process; at the solid boundary, the velocity field has little effect on solute transport, while the osmotic permeation is significantly more effective than molecular diffusion. The concentration boundary layer thickness is, however, controlled by the channel hydrodynamics and is thinner at higher velocities, resulting in a shorter time required for a fully established concentration profile.

An intermediate time-scale which may also be considered, is the time required for diluting the feed channel to an average concentration equal to the bulk concentration. An illustrative example of this may be seen in Fig. 8, where the time evolution of both the average membrane surface concentration, C_m and the domain-averaged concentration, C_d, is shown for two different crossflow velocities. Note that in the present model, at a higher crossflow velocity the domain-average concentration drops only slightly below the bulk concentration, even upon reaching steady conditions.

The performed simulations provide a clear indication that, at short times, the back-flush process is virtually unaffected by the crossflow velocity. During this stage of the cycle, keeping the presence of the feed channel crossflow provides no significant advantage over shutting it down completely. However, it remains to establish what period would qualify as 'short time'. Consider, for example, the time evolution of the permeation rate in the presence and absence of crossflow (Fig. 9). The decline of the osmotic permeation follows similar trends regardless of the presence of crossflow (which, in fact results in a slightly more rapid decline); this situation then changes as the steady state is reached, at which point the no-crossflow case continues to decline. It follows that, for describing the process during its transient stage, the effect of axial advection may be neglected with seemingly little error; this period would correspond with the time T_S, previously defined. The presence of crossflow would become beneficial only in cases where the back-flush is to be carried out for periods greater than T_S, ensuring a maximum cycle-averaged permeation rate, presumably needed for an effective process.

3.5. Osmotic backwashing via a high concentration pulse

Finally, the general characteristics of an alternative backwash configuration are considered. In this case a pulse of a high concentration solution is injected into the feed stream, increasing the osmotic pressure to a level exceeding the applied hydraulic pressure, which remains unchanged [9]. This configuration has the advantage of not disrupting the RO process, in terms of the pressure/flow-rate changes required for initiation of a backwash event. Furthermore, this provides a means for inducing osmotic backwashing in cases where the feed solution itself is incapable of providing the necessary osmotic driving force (e.g. low-salinity brackish/wastewater).

Two limiting cases were considered in our simulations. In the first, a short pulse is introduced into the feed channel, where by 'short' it is understood that the solute residence time in the membrane channel is much longer than the pulse duration. Under such conditions, the pulse propagates through the channel, occupying only a portion of the channel at any given time. Conversely, a long pulse is here defined as one which is of greater duration than the residence time; thus, a concentration front propagates through the channel during the initial transient leading to a fully developed 'diluted' concentration polarization layer. The propagation of the pulse is shown in terms of the axial distribution of the permeation rate, see Fig. 10.

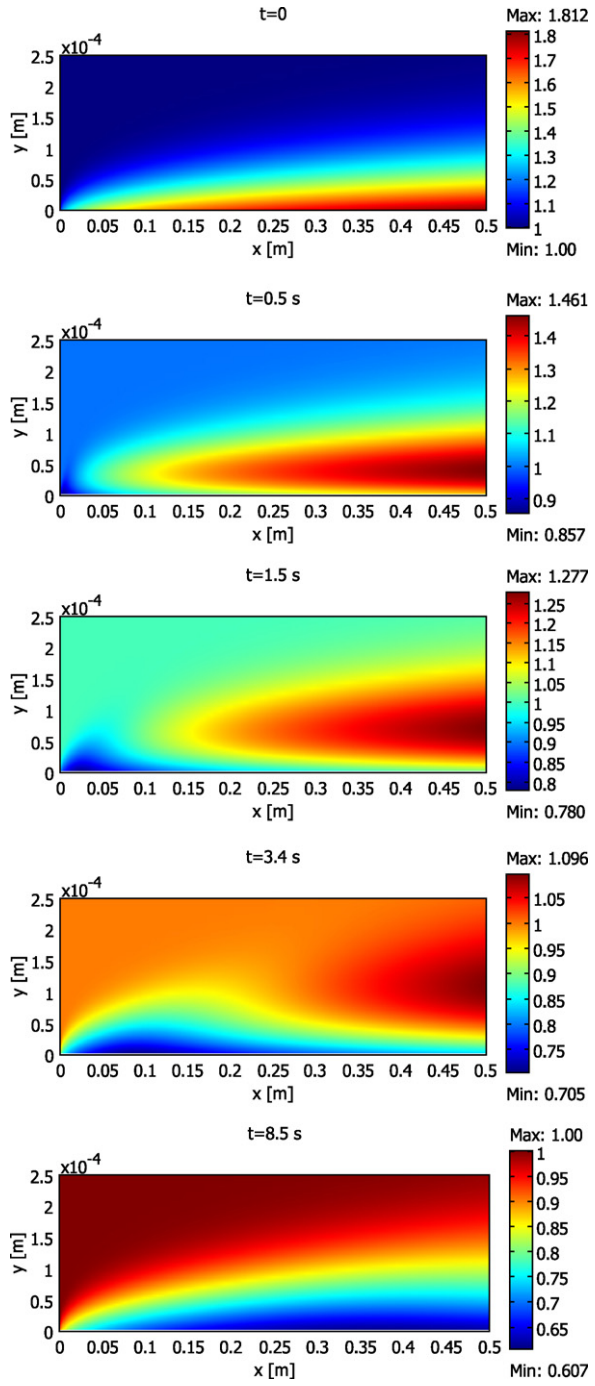

Fig. 6. Transient concentration field, at various times during a complete dilution cycle. Simulations made with a crossflow velocity of $U = 0.25$ m/s. Note the different color coding for each time shown. (For interpretation of the references to color in this figure legend, the reader is referred to the web version of this article.)

In the short pulse case (Fig. 10a), the most striking feature is the spreading of the locally induced osmotic permeation as it propagates along the channel. This is due to the retarding effect of the solid wall (also manifested in the classical case of 'Taylor dispersion'). The spreading is also accompanied by dilution through the osmotic permeation, and results in a pronounced decrease of the effectiveness of the concentration pulse in inducing the back-flow. In the illustrated simulation, by the time the pulse has barely reached the mid-channel (at $t = 10$ s), its concentration is not high enough to induce the desired back-flow (which was quite substantial at the inlet). The strong dilution may also be observed in Fig. 11,

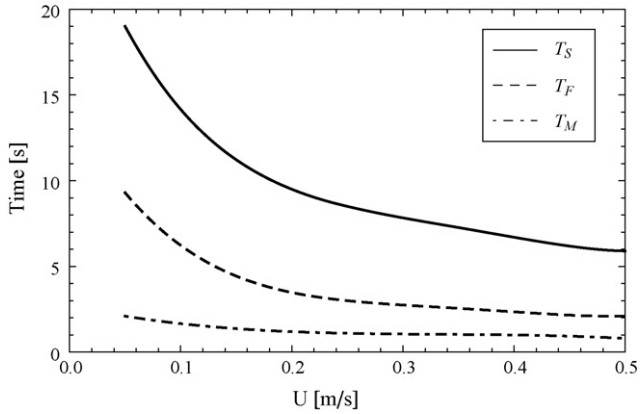

Fig. 7. Characteristic times in a backwash cycle, as a function of the crossflow velocity, U. T_S – time required for reaching a steady state; T_F – time required for 'flattening' of the concentration profile; T_M – time required for membrane surface concentration to reach the bulk value.

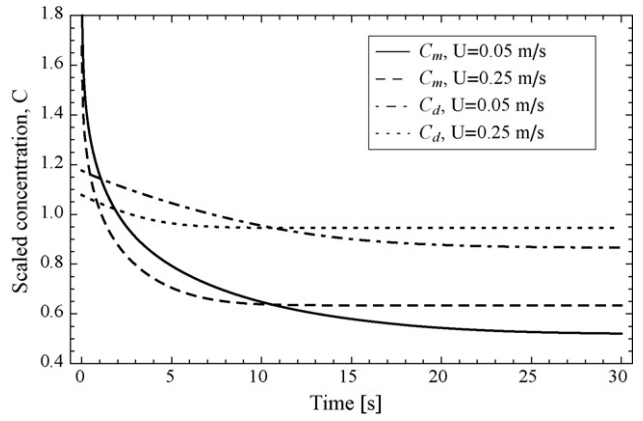

Fig. 8. Time evolution of the channel-average membrane surface concentration, C_m, and the average domain concentration, C_d, calculated for two crossflow velocities.

where the average concentrations at the inlet and outlet have been plotted over time. In the case presented, the peak concentration of the pulse has dropped from 18 times the bulk concentration, to merely 7; the membrane surface concentration drops even lower. Performing a high concentration back-flush on a full scale RO system, Qin et al. [9] measured a nearly threefold decrease in the

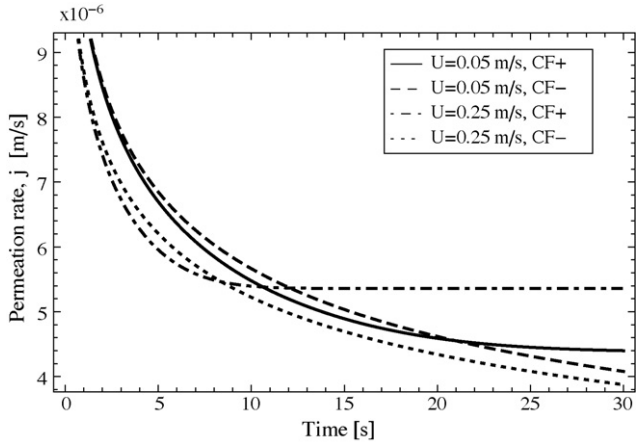

Fig. 9. Time evolution of the channel-average osmotic permeation rate, j, shown with (CF+) and without (CF–) the presence of different values of the crossflow velocity, U.

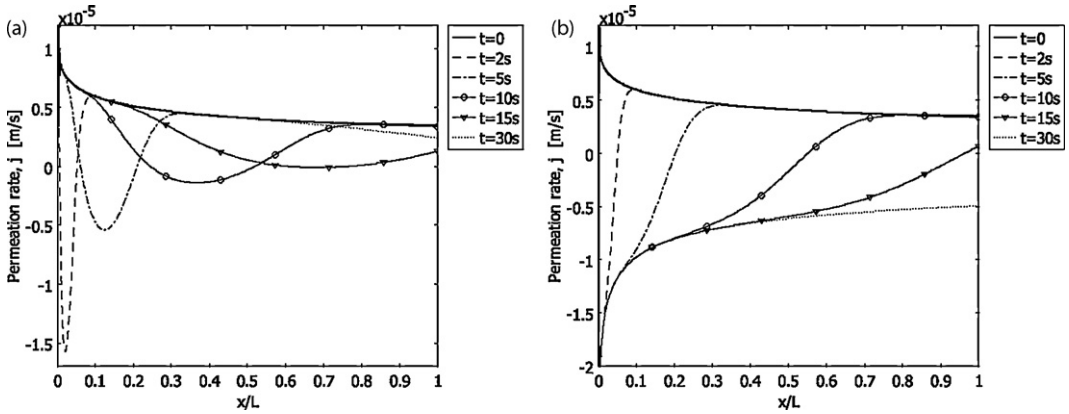

Fig. 10. Spatial distribution of the permeation rate, *j*, in response to an injected pulse of high concentration solution, at various times. (a) 'Short' pulse. (b) 'Long' pulse. The crossflow velocity in both cases is set as $U = 0.05$.

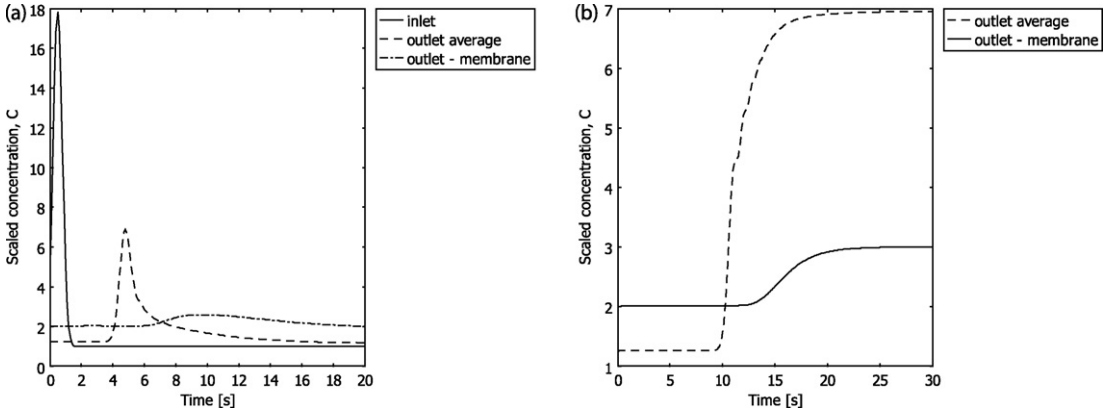

Fig. 11. Transient cross-sectional average concentration at the channel inlet and outlet, during the injection of a high concentration pulse. (a) 'Short' pulse. (b) 'Long' pulse.

peak concentration at the outlet, compared with the inlet. Moreover, measurements of the permeate flow rate clearly indicated that no net flow rate may be osmotically generated for pulse durations below a certain threshold. This corresponds with a situation where dilution renders the injected pulse ineffective as an osmotic draw agent before affecting the full length of the membrane channel. This constitutes a clear disadvantage of such a configuration, with the conclusion that the pulse duration must be a significant fraction of the solute retention time for it to be effective along the entire length of a membrane train. Furthermore, in order to have high back-flow rates at tail membrane elements, the pulse would have to be very concentrated so as to allow for dilution while still retaining enough osmotic potential.

In contrast, a long pulse (Fig. 11b) represents an idealized situation (in the sense that the dilution is minimized), and provides an estimate of the maximum back-flow available along the membrane channel. In the case presented, the permeation rate at the outlet drops roughly fourfold compared with the inlet (we note that the crossflow velocity is set at the relatively low value of 0.05 m/s, so polarization is rather severe). This effect is also seen in terms of the membrane surface concentration at the outlet, compared with the average outlet concentration (Fig. 12). Another point in favor of a long pulse is the desired duration of a backwash event – longer times would require a correspondingly long pulse injection. In their study, Qin et al. [9] observed that the osmotic flow rate increased with a longer pulse duration, until reaching a constant value; according to the model simulations, this corresponds with a fully established concentration field, at the point where the pulse duration is roughly equal to the average solute retention time.

3.6. Practical implications

The two quantities which are expected to have the greatest impact on any backwash process are its duration and magnitude of the induced permeation velocity. This is also expected in the case of the osmotic backwash, where a main drawback is the fact that the process is not externally controlled; rather, it is coupled with the internal dynamics of the concentration field. As already mentioned, there is currently very little data from which the effectiveness of an osmotic-induced backwash may be deduced. It is

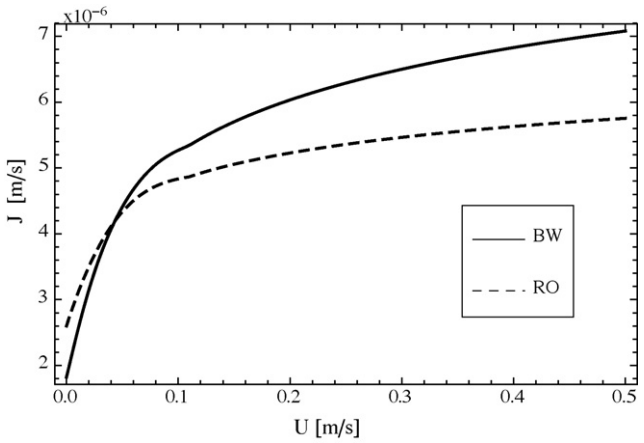

Fig. 12. Averaged permeation rate, *j*, as a function of the crossflow velocity, *U*, calculated for RO and backwash under steady state.

therefore instructive to compare the osmotic permeation rate with backwash velocities used in microfiltration (MF), where backwashing is routinely implemented for fouling control. In general, MF backwash velocities may be an order of magnitude higher than those achievable for RO. Fig. 12 illustrates some characteristic values of the permeation rate achievable in an osmotic backwash, as a function of the applied crossflow velocity; for comparison, calculations of the RO steady-state permeation are also presented. As may be seen, the backwash permeation rate is comparable to, or greater than the RO permeation; calculated values are generally on the order of 5 μm/s, while the initial osmotic permeation rate is substantially higher, on the order of 13–15 μm/s. However, the osmotic permeation rapidly declines and, when averaged over a 30 s period, becomes comparable with the steady-state values.

Although it is difficult to a priori assess the effect of the calculated osmotic permeation on the removal rate of material deposited on the membrane, it has previously been shown that yeast cells were efficiently removed from an MF membrane by back-flushing at a velocity of 9.4 μm/s [12]. The forward flux applied was of identical magnitude, and was identified as being 'sub-critical', in the sense that the overall force balance on a particle (including permeation drag and XDLVO interactions) predicted a reversible deposition (secondary minimum). Under these conditions, cell removal was accomplished at a high rate (94%, increasing to 96% at 28.3 μm/s) during a backwash period of less than 30 s. It therefore appears that, as far as such an analogy can be made, the permeation induced during an osmotic backwash event is favorable when compared with conditions which have been successful in removing cells deposited on an MF membrane. A main difference here, besides the differences in membrane surface properties, is the high ionic strength present at the membrane surface during RO, resulting from concentration polarization. This substantially reduces elecro-static repulsion forces and creates conditions which are more favorable for deposition.

As a final remark, it should be noted that the present model and, indeed, the current literature on osmotic backwashing, does not contain a thorough consideration of the presence of fouling of any kind. The presented model considers only the transient concentration field and, as such, may be regarded as a bench-mark, providing insight to the process dynamics. The efficiency of an osmotic flow in removing various forms of fouling from a membrane surface and, particularly, the possible impact on the permeation rate and time-scales involved, require further experimental work. Furthermore, phenomena such as 'cake-enhanced osmotic pressure' [13], the presence of additional resistances to the permeation and their transient decline due to fouling removal during a backwash event, all pose a formidable modeling challenge. Moreover, it is unclear what effect a reversible mineral scale has on the osmotic driving force. The main challenge stems from the fact that the backwashing process is strongly coupled with its driving force; thus, for example, while the dilution of the concentration at the membrane surface reduces the available driving force, the removal of, say, a biofilm diminishes the hydraulic resistance to the back-flow. These coupled effects represent simultaneously negative and positive feedback loops inherent to the process. Furthermore, the physical–chemical interactions which accompany the detachment, such as charge interactions between colloids/bacteria in a transient solution environment, are of fundamental value in understanding the process and may play a key role in designing an effective backwashing protocol.

4. Summary and concluding remarks

In the presented study, numerical simulations have been performed in order to illustrate the dynamics of an osmotic backwash event during reverse osmosis desalination. For a backwash cycle initiated by reduction of the trans-membrane pressure, various aspects of the concentration field and transport mechanisms have been illustrated and discussed. These include the transient concentration field, characteristic time-scales and the osmotic permeation rate. In addition, the effect of permeate-side concentration polarization on the backwash process was assessed. A representative case was compared with published experimental data, showing excellent agreement.

Results have indicated that at short times, which may loosely be defined as the period of initial detachment of the concentration profile, the osmotic permeation rate is only weakly affected by the presence of the crossflow velocity. At longer times, the presence of a crossflow ensures that a higher permeation rate is maintained. This is of practical significance, indicating a clear advantage for a configuration which allows the continued application of the feed flow rate, particularly where longer backwash events are required; such a configuration would possibly require process modifications to the permeate side, e.g. high pressure tubing. If, on the other hand, a short backwash period is sufficient for membrane cleaning, the presence or absence of a crossflow is of little consequence; in this case, however, the short duration may in itself pose some technical challenges.

An osmotic backwash induced by a high concentration pulse, introduced into the feed channel, has also been briefly considered. Two limiting cases were simulated: that of a short duration pulse, here defined to be much shorter than the mean solute retention time, and a long pulse which enables the establishment of a steady-state concentration field, for which the maximum overall permeation may be induced. Based on the simulations it may be concluded that, due to its dilution, a short pulse may be ineffective in inducing osmotic permeation, particularly toward the end of the channel. These observations are in qualitative agreement with some experimental measurements and suggest that the process must be carefully optimized if efficient osmotic cleaning is to be achieved throughout the full length of a membrane train.

Calculated osmotic permeation rates are generally higher than those present during RO operation and, based on deposition studies performed on MF membranes, should be of sufficient magnitude for removal of deposited material, provided that the deposition is reversible. However, it is still a matter of further investigation to establish the connection between the magnitude of the RO flux and osmotic backwash efficiency. In addition, the present model must be refined so as to include the effect of additional resistances to permeation, arising from the presence of various possible forms of fouling.

Nomenclature

c	concentration [mole/m^3]
C	averaged concentration [mole/m^3]
D_m	molecular diffusion coefficient [m^2/s]
h	half-channel height [m]
j	permeation rate [m^3/m^2 s]
J	channel-averaged permeation rate [m^3/m^2 s]
L	channel length [m]
L_p	membrane permeability coefficient [m^3/m^2 s Pa]
ΔP	trans-membrane pressure [Pa]
R	membrane rejection
R_g	universal gas constant [J/mole K]
t	time [s]
T_F	time required for reaching a 'flattened' concentration profile [s]

T_M	time required for membrane concentration to reach the bulk concentration [s]
T_S	time required for reaching steady state [s]
T	temperature [K]
u	axial velocity component [m/s]
U	centerline velocity [m/s]
v	transverse velocity component [m/s]
x	axial coordinate [m]
y	transverse coordinate [m]
Y	scaled transverse coordinate, y/h

Greek letters

β	osmotic coefficient, $2R_gT$ [J/mole]
Π	osmotic pressure [Pa]

Subscripts

b	bulk
m	membrane
p	permeate

Abbreviations

CP	concentration polarization
RO	reverse osmosis
TMP	trans-membrane pressure, ΔP

References

[1] A. Achilli, T. Cath, A. Childress, Power generation with pressure retarded osmosis: an experimental and theoretical investigation, J. Membr. Sci. 343 (2009) 42–52.
[2] J. Chen, S. Kim, Y. Ting, Optimization of membrane physical and chemical cleaning by a statistically designed approach, J. Membr. Sci. 219 (1–2) (2003) 27–45.
[3] C. Fritzmann, J. Lowenberg, T. Wintgens, T. Melin, State-of-the-art of reverse osmosis desalination, Desalination 216 (2007) 1–76.
[4] S. Chesters, Innovations in the inhibition and cleaning of reverse osmosis membrane scaling and fouling, Desalination 238 (2009) 22–29.
[5] K.S. Spiegler, J.H. Macleish, Molecular (osmotic and electro-osmotic) backwash of cellulose acetate hyperfiltration membranes, J. Membr. Sci. 8 (2) (1981) 173–192.
[6] A. Sagiv, R. Semiat, Backwash of RO spiral wound membranes, Desalination 179 (1–3 Spec. Issues) (2005) 1–9.
[7] N. Avraham, C. Dosoretz, R. Semiat, Osmotic backwash process in RO membranes, Desalination 199 (1–3) (2006) 387–389.
[8] A. Sagiv, N. Avraham, C.G. Dosoretz, R. Semiat, Osmotic backwash mechanism of reverse osmosis membranes, J. Membr. Sci. 322 (1) (2008) 225–233.
[9] J. Qin, H. Oo, K. Kekre, B. Liberman, Development of novel backwash cleaning technique for reverse osmosis in reclamation of secondary effluent, J. Membr. Sci. 346 (2010) 8–14.
[10] W. Zhou, L. Song, Experimental study of water and salt fluxes through reverse osmosis membranes, Environ. Sci. Technol. 39 (2005) 3382–3387.
[11] S. Redkar, V. Kuberkar, R. Davis, Modeling of concentration polarization and depolarization with high-frequency backpulsing, J. Membr. Sci. 121 (2) (1996) 229–242.
[12] S. Wang, G. Guillen, E.M.V. Hoek, Direct observation of microbial adhesion to membranes, Environ. Sci. Technol. 39 (2005) 6461–6469.
[13] E.M.V. Hoek, M. Elimelech, Cake-enhanced concentration polarization: a new fouling mechanism for salt-rejecting membranes, Environ. Sci. Technol. 37 (24) (2003) 5581–5588.